SSC20-P3-15

Power-Optimal Slew Maneuvers in Support of Small Satellite Earth Imaging Missions

Skylar Cox, Tyson Smith, Tanner Lex Jones
Space Dynamics Laboratory
1695 Research Park Way, North Logan, Utah; 435-713-3365
skylar.cox@sdl.usu.edu

Greg Droge
Utah State University
4100 Old Main Hill, Logan, Utah; 435-797-8310
greg.droge@usu.edu

Amber Spackman Jones
Utah Water Research Laboratory
8200 Old Main Hill, Logan, Utah
amber.jones@usu.edu

ABSTRACT

Small satellite image collection missions typically rely on commercial, off-the-shelf products with control systems that use established methods for managing spacecraft attitude operations. Controllers in this marketplace simply move the spacecraft between commanded orientations without considering solar exposure. In particular, performing a specified slew based on traditional methods may keep solar arrays in shadow, draining the satellite's power. To compensate, satellite operation teams often command the vehicle to enter a "sunbathe" state between collections. This additional level of complexity requires manual or rigidly prescribed specification of the frequency and duration of the "sunbathe" operation. However, there is opportunity for power collection during movement if satellite slews are controlled to optimize solar exposure in combination with control input. This paper describes development of a novel satellite slew maneuvering controller that optimizes satellite power state. By controlling reaction wheel accelerations and orienting solar arrays during slew maneuvers, opportunities for both image collection and power collection and consumption are considered. The controller reduces the need for operator decisions by integrating power collection with imaging tasks. This approach first prioritizes several image collection targets using an image collection score and slew cost in discretized time to generate a directed acyclic graph. The optimal collection path through the graph is then computed to generate a representative slew plan for the power state optimal controller. In simulation of several scenarios, satellite behavior reflected power-prioritized objectives while achieving collection requirements. Performance of the power-optimal controller was compared with a standard small satellite controller to evaluate both power state and attitude during collections. The power-optimal system resulted in equal collection performance while ensuring a more power-positive state for the spacecraft but required greater maximum power input and greater overall computational cost. The power-optimal controller has direct application to small satellite earth imaging missions that are often power constrained due to non-articulated solar arrays and relatively small power storage capacity.

1 Introduction

Earth imaging from space-based platforms began over 50 years ago and has since increased dramatically.[1] Today, imaging satellites number in the thousands and orbit our world many times each day. While Earth imaging was initially only a government endeavor,[2] it is now the focus of a commercial marketplace offering affordable data for a variety of sectors, including archaeology,[3] investment,[4] natural disaster recovery,[5] and insurance.[6] Commercial companies currently operate constellations of satellites dedicated to Earth imaging and innovative new business applications.[7] While many government satellite systems have grown in size and complexity, commercial satellites are shifting toward smaller

and more affordable designs. Earth imaging missions, previously handled by larger space vehicles, are increasingly being carried out by constellations of smaller satellites. Due to their sheer numbers, multiple small satellites working in tandem outperform larger systems in terms of Earth surface coverage and revisit rate.

Attitude management for small satellites is generally performed by off-the-shelf control systems that are integrated with the vehicle.[8] These control systems move the spacecraft directly between orientations for image collection targets and other commanded alignments. Small satellites are typically designed with fixed solar arrays, and solar exposure for power collection is considered separately from imaging operations. As a result, a typical slew between targets can deplete power resources as solar arrays are rotated away from the sun.[9] To maintain a power-positive state, mission operators often command sunbathe orientations (arrays pointing toward the sun) between image collection activities. Due to the relatively low power storage capacity of small satellites, frequent sunbathe operations detract from image collection capabilities.[10] Determination of the duration and frequency of the sunbathe operation is either performed manually or by a predefined and rigidly prescribed set of rules.[9] By coordinating satellite slews to optimize solar exposure, there is opportunity to integrate power collection with imaging operations.

Currently, within a specified trajectory for a small satellite, reaction wheels are typically used to perform slews to direct orientation for image collection.[8] Several control methods have been proposed to direct satellite slewing, including time-optimal, torque-optimal (also known as control input-optimal), and minimal instantaneous power. Time-optimal is a common method for attitude control that prioritizes image collection by minimizing the time to perform the slew between image captures.[11][12] In efforts to push the envelope in speed improvement for reaction wheel spacecraft, Karpenko and King proposed maximizing "agility envelopes," which refers to slewing the satellite in the direction of least resistance as opposed to the most direct path.[13] Time-optimal methods, while ensuring the most possible target collections, expend as much power as necessary until forced into an idle sunbathe orientation to recharge satellite batteries. This control strategy is also discouraged because it causes vibration in the spacecraft unless augmented by a smoothing optimization.[14] Another important consideration for all satellite slewing operations is the torque limitation of conventional reaction wheels. Torque-optimal control considers the power consumption of the reaction wheels and minimizes the input torque. This approach is slow relative to the time-optimal method, but it expends less power to execute the slew. Several methods have been investigated to achieve this solution.[15] Schaub described a related approach to minimize instantaneous power usage rather than the torque of the slew.[16] This approach may utilize more wheel torque than the torque-optimal method but was determined to be more effective at power conservation. Power regeneration has also been considered to this end.[17] These existing methods implement satellite control to conserve power, but so far as we know, this is the first approach for small satellite attitude control that optimizes satellite power state or that accounts for solar orientation in a slew.

In this paper, a novel controller for satellite slew maneuvering with a control law that prioritizes satellite power state is described. Rather than emphasizing efficiency in time/space (time-optimal) or efficiency in power usage (control input-optimal), the power-optimal control considers both image and power collection. To accomplish this, an optimal image collection plan and schedule are developed. The satellite executes the plan by controlling reaction wheel accelerations to orient solar arrays during slew maneuvers when power collection may be profitable. Section 2 describes challenges and approaches to planning for collection of multiple ground targets and the proposed solution for schedule generation and operation before considering power input. Section 3 defines the power state optimal control law including related details for power consumption (control input/reaction wheel) and power collection (solar array orientation). Section 4 reports a full orbital integrated simulation of the power-optimal control with a prescribed collection target deck, spacecraft orbit, selected plan, power state, and pointing performance. Performance is assessed and compared with a reference controller. Section 5 presents the observed results and suggestions for future investigation.

2 Collection Planning Operations

Optimizing collection of a set of imaging targets is essential to meeting the operational goals of a satellite system. A complete space system architecture consists of several components including: 1. *Tasking*: ground images are specified and requested for imaging, 2. *Collection Planning*: a mission planner generates an optimal schedule of collections, 3. *Execution*: satellites collect images, and 4. *Data De-*

livery: collected images are received, processed, and delivered to the customer. Under planning of satellite collection operations, a schedule of sensor angles corresponding to each target collection is generated. These angles are used as the terminal points for executing the power-optimal control solution. We created an objective function for a single satellite that considers the value of a particular imaging target and the associated cost with collection. Imaging targets, and their priority scores, are specified by the customer and are then adjusted based on factors that impact the collection value including quantities such as geometry, cloud cover, urgency, and snow cover. We define collection cost as slew angle multiplied by the inverse of the time required. The difference between the value and the cost yields the objective score for each collection.

2.1 Planning Formulation Background

Several methods exist for planning satellite collections. The knapsack approach formulated by Vasquez and Hao includes tasks on the schedule ("knapsack") that maximize the target value while staying within the satellite's memory capacity.[18] Using a tabu search algorithm yielded good schedules but was computationally expensive, and optimality was difficult to predict. Incorporating the limitations of downlink connection in which a satellite must compete to transmit data to a ground antenna, Song et al. implemented a Hybrid Genetic Algorithm to successfully solve the oversubscribed scheduling problem.[19] Augenstein et al. considered both task collection as well as data downlink using dynamic programming.[20] Their approach computes access to available targets and discretizes through time to build a graph with connections that represent valid slew paths within the time constraints. Due to discretization, the resulting schedule may not be optimal but approximates optimal paths. For this work, we follow a similar approach that generates possible paths to capture targets with consideration for solar exposure. Downlink planning is left to later efforts.

2.2 Planning Solution

To generate a collection plan, image targets are discretized into time windows of collection opportunities. Each opportunity becomes a node of a directed acyclic graph (DAG) through which the optimal path is found. This general approach is illustrated in Figure 1. The method first determines when a satellite has a valid collection opportunity based on geometry and lighting constraints. With that information, the planning routine determines if it is possible to slew between two targets by calculating the worst-case angle between the two collects and dividing that by the satellite's slew agility. This yields a conservative estimate of how long the slew will take. That conservative slew duration is compared to the time between the two collection opportunities. If there is sufficient time between those collection tasks to perform the slew, a connection between targets is added to the DAG. A path is then determined by optimizing over the DAG, similar to Augenstein et al.[20] There may be multiple nodes for each target when the opportunity for collection spans multiple time windows. For example, if target A can be collected at 2 distinct time steps, it is allotted 2 nodes in the graph. Note that each target grouping (e.g., cluster of A nodes) is constrained to have only one exit path selected during the optimization. This prevents the algorithm from attempting to slew back to a target that it has already collected (e.g., A-C-A) due to the time discretization routine (creating multiple nodes of a single geographical target).

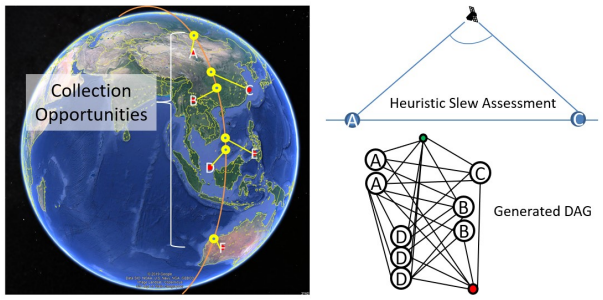

Figure 1: Representation of a collection planning DAG using target opportunity time discretization and heuristic slew assessment. Opportunities are first calculated (left) and then discretized. A slew heuristic (top right) is then used to determine valid connections between nodes (bottom right).

The DAG optimization routine determines the overall cost-optimized path to fulfill collection opportunities where the optimized objective function is the difference of the slew cost and the associated target value. The value of a target is calculated using a customer-defined priority score multiplied by the cloud cover ratio, the cosine of the perspective angle, and similar penalties to account for any other mitigating factors. The slew cost is a function of slew angle and time expense. Time expense corresponds to the maximum allowable time to complete the slew and still collect the image within the time window, which minimizes power consumption. With

the value and costs established and the DAG generated, the optimization routine is run to identify an optimal collection plan. For this step we use the Matlab optimization toolbox. An example DAG and optimal collection plan are shown in Figure 2. The collection plan results in a sequence of targets and collection times that are given to the controller for execution. The nodes in the target plan establish the initial and terminal conditions for each slew.

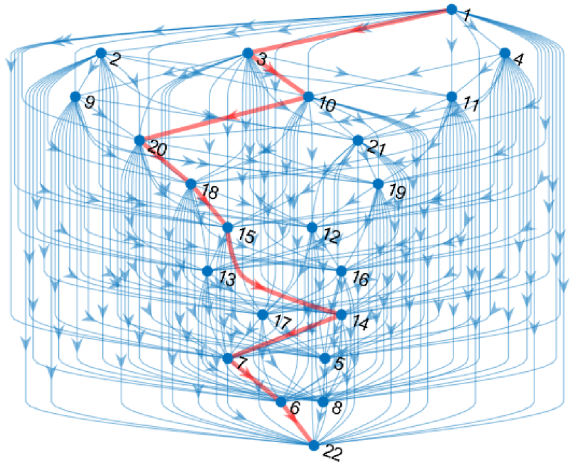

Figure 2: Example of a collection planning DAG connecting target opportunities. Blue lines represent feasible paths between time-target pairs based the slew time assessments. The optimal collection path is highlighted red.

3 Slew Maneuver Control

To optimize power state during a slew maneuver, momentum wheel acceleration is controlled to orient the spacecraft solar arrays for maximum power collection. This section outlines the system dynamics that define the solution space for this optimization problem, presents the cost function, and states the chosen method for discrete simulation.

3.1 State Dynamics and Jacobian Formulation

Slew maneuvers can be formulated for a vehicle constrained to one axis of orientation as the vehicle moves along a circular orbit. The state of the system is defined by Equation 1:

$$x = \begin{bmatrix} \omega_w \\ \theta_{sc} \\ \omega_{sc} \\ \nu \end{bmatrix} = \begin{bmatrix} x_1 \\ x_2 \\ x_3 \\ x_4 \end{bmatrix}, \tag{1}$$

where ω_w is the angular velocity of the momentum wheel, θ_{sc} is the angular position of the spacecraft, ω_{sc} is the angular velocity of the spacecraft, and ν represents the true anomaly, or the angular position of the spacecraft along its orbital path. Figure 3 illustrates how ν and θ_{sc} are defined. ν is calculated by Equation 2.

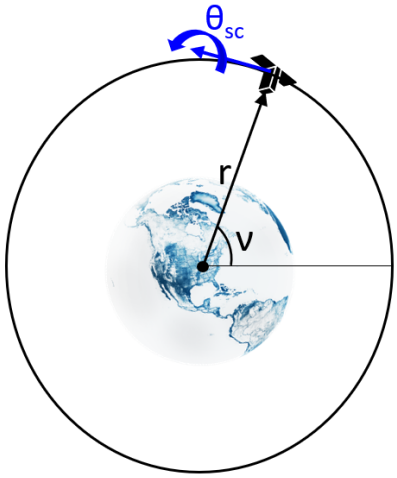

Figure 3: Illustration of satellite orbital position vector, true anomaly (ν), and the spacecraft angular position (θ_{sc}).

$$\nu = \frac{2\pi}{T_p} t \tag{2}$$

In Equation 2, t represents the time since the spacecraft passed perigee ($\nu = 0°$), and T_p is the period of the orbit, given by Equation 3:

$$T_p = \frac{2\pi}{\sqrt{\mu}} r^{3/2}, \tag{3}$$

where μ is the Earth's gravitational constant $\left(398600 \frac{km^3}{s^2}\right)$, and r is the radius of the orbit.[21] The control input, u, of this system is the angular acceleration of the momentum wheel α_w (Equation 4).

$$u = \alpha_w \tag{4}$$

The instantaneous power collected by the spacecraft, P_c, is defined by Equation 5:

$$P_c = P_s \psi, \tag{5}$$

where ψ is dependent on the angle between the spacecraft's solar array normal vector and the sun vector derived below. P_s is the solar power available to the satellite for collection given by Equation 6:

$$P_s = S_a A_{panel} F_{solar}, \tag{6}$$

where S_a is a unit-less ratio between 0-1 representing the available sunlight due to eclipse from Earth's shadow, A_{panel} is the area of the solar panels, and F_{solar} is the average annual solar radiation arriving at the top of Earth's atmosphere $\left(\approx 1361 \frac{W}{m^2}\right)$. For this analysis, a simple model is used to calculate ψ as a function of the true anomaly, ν, and angular position of the spacecraft, θ_{sc}. The value for ψ is derived by projecting these two angles into the sun vector.[21] The projection of ν into the sun vector is calculated by Equation 7:

$$c_\nu = |a_\nu||b_\nu| cos(\nu), \tag{7}$$

where a_ν is a unit vector in the direction of ν, b_ν is a unit vector in the direction of the sun, and c_ν is the projection of a_ν into b_ν. Projecting θ_{sc} into c_ν gives ψ (Equation 8), which is expanded in Equation 9:

$$\psi = |a_{\theta_{sc}}||c_\nu| cos(\theta_{sc}) \tag{8}$$

$$\psi = |a_{\theta_{sc}}||a_\nu||b_\nu| cos(\nu) cos(\theta_{sc}), \tag{9}$$

where $a_{\theta_{sc}}$ is the unit vector in the direction of θ. a_ν, b_ν and $a_{\theta_{sc}}$ have magnitudes of 1, therefore Equation 9 is simplified to Equation 10:

$$\psi = cos(\nu) cos(\theta_{sc}). \tag{10}$$

The dynamics of the system are computed by taking the derivative of the state with respect to time (Equations 11 and 14):

$$\dot{x} = \begin{bmatrix} \alpha_w \\ \omega_{sc} \\ \alpha_{sc} \\ \dot{\nu} \end{bmatrix} = f, \tag{11}$$

where α_w is the angular acceleration of the wheel and α_{sc} is the angular acceleration of the spacecraft, which can be calculated by Equation 12:

$$\alpha_{sc} = -\frac{I_w}{I_{sc}} \alpha_w, \tag{12}$$

where I_{sc} is the spacecraft mass moment of inertia about the axis of rotation, and I_w is the wheel's mass moment of inertia.[22] $\dot{\nu}$ is the angular velocity of the orbit and is defined by Equation 13:[21]

$$\dot{\nu} = \sqrt{\frac{\mu}{r^3}}, \tag{13}$$

where r is the orbital radius, and μ is the standard gravitational parameter for Earth. The power output of the system is given by Equation 14:

$$g = \begin{cases} P_s \psi & if\ \psi \geq 0 \\ 0 & otherwise, \end{cases} \tag{14}$$

The case where g = 0 corresponds to solar panels oriented away from the sun. This was accounted for in simulation software, but this case is not explicitly included in subsequent derivation of Jacobian matrices. The system can be rewritten as a function of state x and control u (Equations 15 and 16)

$$f(x,u) = \begin{bmatrix} u \\ x_3 \\ -\frac{I_w}{I_{sc}} u \\ \sqrt{\frac{\mu}{r^3}} \end{bmatrix} \tag{15}$$

$$g(x,u) = \left[P_s cos(x_4) cos(x_2) \right] \tag{16}$$

Note that the dynamics are separable into two distinct systems as x_4 does not affect the first three states and vice versa. Let the first three states be denoted as $x' = \begin{bmatrix} x_1 & x_2 & x_3 \end{bmatrix}^T$. Using Equation 15, the dynamics for x' can be expressed as a linear, time-invariant system of the form

$$\dot{x}' = Ax' + Bu,\ A = \begin{bmatrix} 0 & 0 & 0 \\ 0 & 0 & 1 \\ 0 & 0 & 0 \end{bmatrix},\ B = \begin{bmatrix} 1 \\ 0 \\ -\frac{I_w}{I_{sc}} \end{bmatrix}. \tag{17}$$

Since x_4 is uncontrolled, it can be directly integrated and expressed as a function of time:

$$x_4(t) = x_4(t_0) + t\sqrt{\frac{\mu}{r^3}}. \tag{18}$$

A multiple shooting, direct method for optimal control will be employed as described in Section 4. An essential element of direct methods is that the dynamics need to be discretized.[23] A discrete time step, k, can be associated with the system such that $t = dt * k + t_0$ and $x_k = x(dt * k + t_0)$, and $u_k = u(dt * k + t_0)$, where dt is the time interval between discrete time steps. The discrete time update dynamics for the linear system can be expressed using an exact discretization,[24] of the form

$$x'_{k+1} = \bar{A} x'_k + \bar{B} u_k,\ \bar{A} = e^{Adt},\ \bar{B} = \int_0^{dt} e^{A(dt-\tau)} d\tau B. \tag{19}$$

Similarly, x_4 can be calculated discretely as

$$x_{4_{k+1}} = x_{4_k} + dt\sqrt{\frac{\mu}{r^3}}. \tag{20}$$

3.2 Power State Optimal Control Formulation

Given the defined system dynamics, the power state optimal control problem is defined by formulating a cost based on power state and using a controller to minimize the power usage. To ensure the high precision necessary for Earth imaging from space, a constraint is added to the problem so that $\theta_{sc}(t_f) = \theta_d$, the desired slew angle.

The charge state of the battery at time t can be defined as

$$P_b(t) = P_b(t_0) + \int_{t_0}^{t} (P_c(\tau) - P_u(\tau))d\tau, \tag{21}$$

where t_0 is the initial time of the slew maneuver, $P_u(\tau)$ represents the instantaneous power used by the reaction wheel, and $P_c(\tau)$ denotes the instantaneous power collected by the solar arrays. The power used can be calculated by

$$P_u = C\alpha_w + P_n, \tag{22}$$

where C is an empirically determined constant, and P_n is the nominal electrical power use of the satellite.

The objective to be minimized is taken as the negative of the charge state at time t_f, i.e., $\min J = -P_b(t_f)$. As mentioned, the direct aspect of this approach assumes that the dynamics and cost are discretized. The multiple-shooting component of the formulation introduces the state variables as parameters of optimization through the introduction of slack variables and the use of the dynamic constraint. To discretize the final time, a final step can be calculated as $N = (t_f - t_0)dt$. The final charge state of the battery is then written as P_{b_N}. This allows the problem to be expressed as

$$\begin{aligned} \min_{x_k,k=1,\ldots,N;u_k,k=0,\ldots,N-1} & J(x_N) = -P_{b_N} \\ \text{s.t. } & x'_{k+1} = \bar{A}x'_k + \bar{B}u_k \\ & x_{4_{k+1}} = x_{4_k} + dt\sqrt{\frac{\mu}{r^3}} \\ & x_{2_N} = \theta_d \end{aligned} \tag{23}$$

The final constraint in Equation 23 can cause the numerics of the optimization to quickly get stuck in an undesirable local minimum. Thus, a warm start is given by first optimizing a problem where the final state constraint is removed and weighted objective $J_i(x_N)$ is formulated as

$$\begin{aligned} & \min_{x_k,k=1,\ldots,N;u_k,k=0,\ldots,N-1} J_i(x_N) \\ & = -C_P P_{b_N} + C_\theta (x_{2_N} - \theta_d)^2 \\ & \text{s.t. } x'_{k+1} = \bar{A}x'_k + \bar{B}u_k \\ & x_{4_{k+1}} = x_{4_k} + dt\sqrt{\frac{\mu}{r^3}} \end{aligned} , \tag{24}$$

where C_P and C_θ are weighting factors. The resulting solution is then fed into the initial guess for the parameters when solving $J(x_N)$ in Equation 23.

4 Case Study

To assess performance of the power state optimal control law, sun synchronous orbit was selected as a case study for initial simulation. With a dawn-dusk sun synchronous orbit, the orbit plane of the satellite is perpendicular to the sun vector (see Figure 4) so that full solar charging is always available. As a result, we can make simplifying assumptions and illustrate the performance of the power-optimal control law by examining satellite trajectories as it slews for both image collection and charging. We simulated a satellite in sun synchronous orbit for the power state optimal control law and for the traditional approach to compare net power collection during imaging tasks. Three slew maneuvers were executed in simulation to test the performance of the power-optimal control law. The power charge level, angular position and velocity of the satellite, and the angular acceleration of the reaction wheel were examined through the duration of the simulation. In addition to simulating these three slews, we also compared the power-optimal control law to a standard implementation of control for an image collection plan consisting of several target-time pairs. The following sections describe the methodology and parameterization of the simulation. Note that all optimization was implemented in MATLAB using the MATLAB Optimization Toolbox.

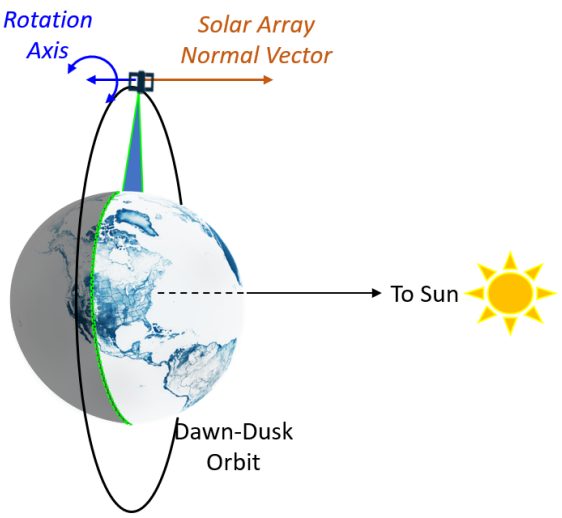

Figure 4: Illustration of satellite orbit and spacecraft rotation axis relative to orbit position.

4.1 Mechanics of Sun-Synchronous Orbit

For sun-synchronous orbits, the orbital plane maintains a constant orbital beta angle relative to the sun vector by rotating in inertial space at the same rate as the angular velocity of Earth's orbit around the sun, or 360° per 365.26 days (0.9856° per day). Because the orbital plane precesses at the same rate as Earth's rotation with respect to the sun, the Right Ascension of the Ascending Node (RAAN) will lie at a fixed local time. The satellite passes over the same location on Earth at nearly the same time of day, day after day.[21]

4.1.1 Dawn-Dusk Orbit

A dawn-dusk orbit is a special type of sun-synchronous orbit that keeps the satellite directly above an area of Earth in sunrise or sunset (Figure 4). In this orbit, the solar panels of the satellite can always be aligned perpendicular to the sun vector for maximum solar power collection.[21] A dawn-dusk orbit aligns the orbit's RAAN with the Earth terminator. Because the sun is always available, a dawn-dusk orbit was selected for simulation with the optimal power controller to assess algorithm performance without concern for satellite states in eclipse.

4.2 Simplified Power Model for the Dawn-Dusk Case

For the dawn-dusk case, the sun vector is constant relative to the orbit plane, so the spacecraft position within the orbit, ν, does not need to be accounted for in the dynamics. Thus, Equation 10 can be simplified to:

$$\psi = cos(\theta_{sc}), \tag{25}$$

For this chosen orbit, eclipse is not possible, so $S_a = 1$. This simplifies Equation 6 to:

$$P_s = A_{panel} F_{solar}. \tag{26}$$

The power output of the system remains as expressed in Equation 14.

4.3 Spacecraft Parameters

For all scenarios, realistic small spacecraft systems were modeled to provide a basis for an actual mission application with feasible results. These values were in-family with other small satellites developed at the Space Dynamics Laboratory or were conservative estimates based on author experience and refinements through simulation. The parameters described in Table 1 were used.

Table 1: Simulation Parameters

Description	Notation	Value	Units
S/C MOI	I_{sc}	0.16	$kg\ m^2$
RW MOI	I_w	4×10^{-4}	$kg\ m^2$
Solar Array Area	A_{panel}	0.18	m^2
Battery capacity	$\max(P_b)$	200	$W\text{-}hrs$
S/C nominal power use	P_n	15	W
Input limit	$\max(\lvert\alpha_w\rvert)$	50	rad/s^2
RW rate limit	$\max(\lvert\omega_w\rvert)$	733	rad/s
Initial battery charge	$P_b(t_0)$	0.5	N/A
Power weighting coefficient	C_P	0.9	N/A
Time step	dt	0.2	s

4.4 Slew Maneuver Scenarios

To illustrate satellite behavior under power state optimal control, we implemented three slew maneuvers to represent scenarios corresponding to boundary conditions for sunbathing and image collection as endpoints. The first case, *Pass through zero*, represents conditions where the satellite slews through the optimal sun pointing angle on its way to execute a collection task. The optimal controller delays the satellite's progression towards the planned collection point in order to spend additional time in the full sun configuration. The *Zero and back* scenario defines a case where the satellite slews away from the next imaging collection location to maximize power collection before slewing to perform the collection at the specified time. The *Skip zero* scenario conditions are similar to that of the *Zero and back* case, except that dynamic constraints result in insufficient time

to execute a slew to both full sun and to the next collection task. As a result, the power state optimal controller slews directly to the next task.

4.5 Collection Operation Comparison

Beyond the scenarios that simulate slew maneuvers based on specified trajectory endpoints, Earth imaging was simulated using a plan of collection targets and compared to a standard linear slew based on a dawn-dusk orbit. In addition to the parameterization of the system, for this simulation, $\theta_{sc} = \frac{\pi}{2} \pm 1 \times 10^{-3}\ rad$ was set as a keep-out zone to prevent sensor damage by direct solar exposure. Furthermore, the angle of orientation for the imaging sensor was set to point at the center of Earth when the solar panels were aligned for maximum solar collection, $\theta_{sc} = 0$ (i.e., the sun vector is orthogonal to the earth for the dawn-dusk orbit), as shown in Figure 5.

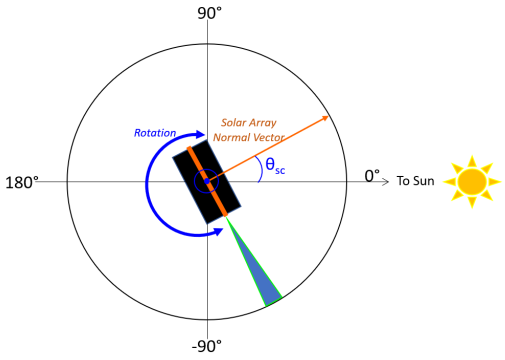

Figure 5: Spacecraft rotation frame and defined measurement of θ_{sc} relative to sun vector.

5 Results and Discussion

This section presents the results of simulations for satellite slewing scenarios (*Pass Through Zero*, *Zero and Back*, and *Skip Zero*) and compares the performance of the power state optimal controller and a standard small satellite control system (*Collection Operation Comparison*).

5.1 Pass Through Zero Maneuver

The *Pass Through Zero* scenario commands the satellite to slew from 90° to −90°, causing θ_{sc} to pass through the maximum solar collection angle. Under the power-optimal control, if the slew duration is long enough, the spacecraft will rotate to 0°, and sunbathe, before rotating to the commanded orientation, as shown in Figure 5. An alternative would be for the satellite to slew through 180° since the slew angle is equivalent. However, in so doing the satellite would lose any power collection opportunity. Figure 6 shows the results from the simulation performing this rotation. The optimal trajectory passes through $\theta_{sc} = 0$ in panel (b). As the satellite performs the maneuver, it first slews to the maximum solar collection angle and remains there (from approximately 10 seconds until 50 seconds) before it moves on to the commanded collection task. To further prove the concept for the *Pass Through Zero* scenario, a similar slew was simulated between 135° and 225° (Figure 7). In this case, however, the two paths between the start and end of the slew are not equivalent, so the power-optimal controller considers power consumed by slewing in either direction with power gained by slewing through 0°, the longer route. Results show that the optimal controller selects the longer slew to drive the satellite through the optimal power-collection orientation (0°) prior to pointing at the commanded location for target collection. The controller opted for the longer route because there was sufficient time to enter full sun for power collection. By taking the spacecraft through $\theta_{sc} = 0$, the predicted charge state increases (+0.36% for a 20-second slew) as opposed to a decrease (-0.1% for a 20-second slew) when taking the shorter route through $\theta_{sc} = 180$. The satellite power state shown in (a) illustrates a strong positive power trend, whereas the direct slew shows a decreasing power state of the vehicle.

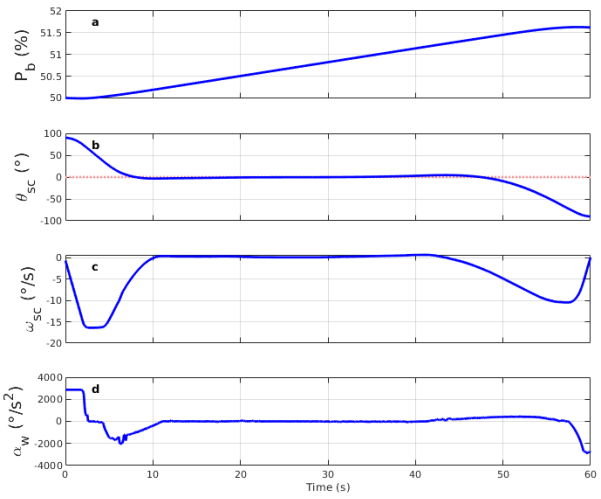

Figure 6: Satellite system states and input for the "Pass through zero" scenario for slewing between 90° and target at −90° (b). System states are satellite battery charge (a), satellite angular position θ_{sc} (b), and satellite angular velocity ω_{sc} (c). Input is reaction wheel acceleration α_w (d). For panel (b), the dashed red line represents the maximum solar collection angle (0°).

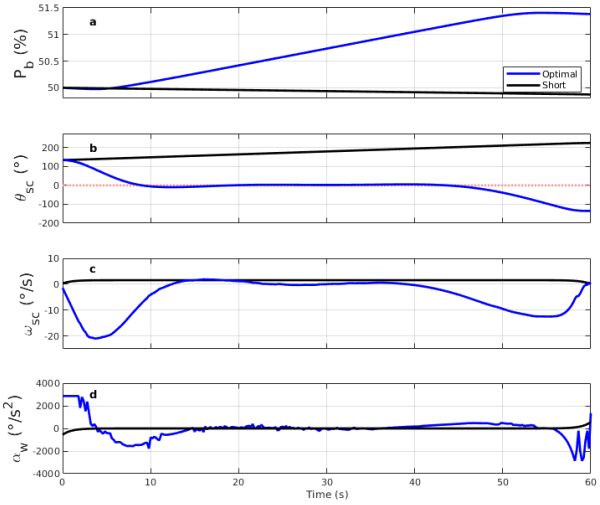

Figure 7: Comparison of a path for optimal power state ("Optimal") with a direct path that disregards power collection ("Short"). See Figure 6 for explanation of panels and axes. Slew begins at 135° and terminates at 225° (reference panel b). For panel b, the two trajectory endpoints are equivalent (225° = −135°).

5.2 Zero and Back Maneuver

The purpose of the "Zero and Back Maneuver" scenario is to evaluate the behavior of the power state optimal controller in selecting to slew directly to a target versus slewing away from the planned target in order to enter full-sun collection conditions. The conditions simulated and evaluated in this paper start the satellite at 45° and then command it to collect a target at 180°.

This scenario should cause the power-state optimal controller to drive the satellite to slew to 0° from the 45° start only if given enough time to rotate back to 180° and collect the target. For this case, we used 60 seconds as the available duration for slewing. Figure 8 shows the results of performing this simulation under the specified conditions. The satellite slewed directly away from the target location (180°) in order to enter full sun collection and then slewed back through its starting point (45°) in order to collect the commanded target at 180°. A standard controller would require a manually-inserted sun-bathe command to generate this type of behavior whereas the power state optimal controller automatically factors these conditions in as part of its normal behavior.

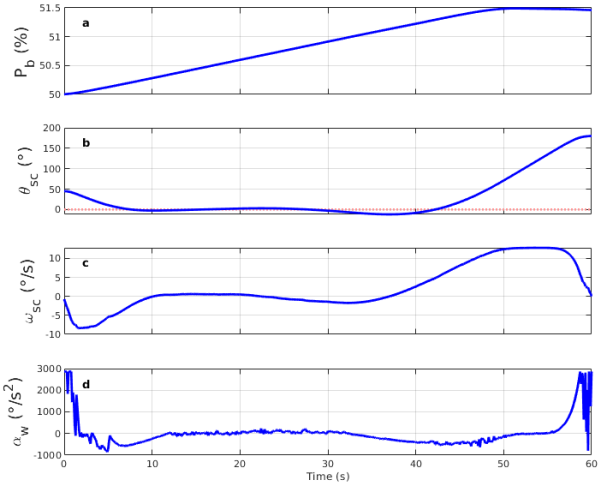

Figure 8: *Zero and back* scenario for slewing between 45° and target at 180° (b). See Figure 6 for explanation of panels and axes.

5.3 Skip Zero Slew Maneuver

The limits of hardware and system dynamics constrain the potential acceleration of spacecraft slewing so that there is insufficient time to slew from starting position, to the maximum power collection position, and then to the commanded target location given the limited reaction wheel acceleration. For this case, the same starting and ending orientations

were used as in Section 5.2, but allowable slew time was reduced from 60 seconds to 10 seconds. The controller must evaluate the input required to drive the satellite to full-sun and then on to the target as opposed to directly driving to the target. With limited allowable slew time, the satellite must input a relatively large amount of power into the reaction wheels, potentially exceeding the allowable acceleration, and make it up while sitting in full-sun before returning to the commanded position.

Figure 9 shows the results from a simulation performing the slew maneuver from 45° to 180° in 10 seconds. The spacecraft is unable to insert a maneuver to full-sun position and instead drives directly to the target (180°). This occurred because slewing to full-sun position was either not power state optimal and would leave the vehicle in a lower power condition compared to slewing directly to the target, or the required acceleration would exceed the allowable acceleration on the wheels. Either condition is properly evaluated by the power state optimal controller.

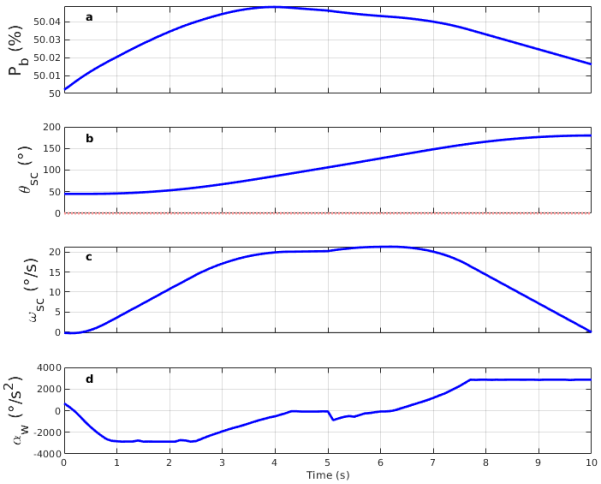

Figure 9: *Skip zero* scenario for slewing between 45° and target at 180° (b). See Figure 6 for explanation of panels and axes.

As shown in Figure 9, if the spacecraft does not have enough time to rotate to 0° and then to 180°, it will rotate directly to 180°.

5.4 Collection Operation Comparison

The results of the comparison of the power state optimal control law and a standard control law is plotted in Figure 10. Using the power state optimal control law resulted in approximately 16% greater net charging throughout the collection period. The standard control law implemented for this simulation moved the satellite over approximately linear trajectories, resulting in small input values (α_w in Equation 4) and decreased maximum velocities. The curved angular position trajectories generated by power state power-optimal control kept the satellite close to the maximum solar collection angle for as much time as possible given the targets and constraints of the system, which resulted in increased charge state relative to the standard control law.

Further comparison shows the computational requirements of the optimization. Every slew was optimized first with the terminal state as a factor of the overall cost; and then after constraining the terminal state, optimization was repeated. The power-optimal trajectories required 6.3×10^5 function evaluations for unconstrained, and 1.1×10^6 function evaluations for the constrained optimization while the standard trajectories required only 2.4×10^4 and 4.1×10^4 evaluations. For this simulation, the power state optimal control optimization had a computational expense approximately 27 times that of the standard controller optimization. The amount of computation would be greatly reduced by solving the cost and constraint gradients, which is beyond the scope of this paper.

6 Conclusion

Satellite imaging supports a variety of diverse purposes and industries, and commercial companies continue to improve on the sensors, systems, and methods employed in their businesses. This study developed a method for satellite image capture planning that incorporates and prioritizes solar charging as part of satellite slew maneuvering between a series of image targets. Power state is optimized through controlling momentum wheel acceleration and orientation of the solar arrays during slew maneuvers. This power state optimal control law was implemented by determining a minimum cost trajectory for a set of targets where cost corresponds to net power. To simulate a satellite controlled by this law, dynamics were derived for satellite slewing on a single axis of rotation for a general circular orbit. As a case study to test the optimal control law, we simulated image collection for a dawn-dusk sun synchronous satellite orbit, examined slewing scenarios, and compared results with a standard controller. Results show that the power state optimal control law collected 16% more solar power than the standard throughout the simulated image capture plan. Furthermore, for each slew between targets, the net power generation of the power-optimal controller was greater than or equal to the standard controller. Because of increased reaction wheel movement to orient toward the sun, the power state op-

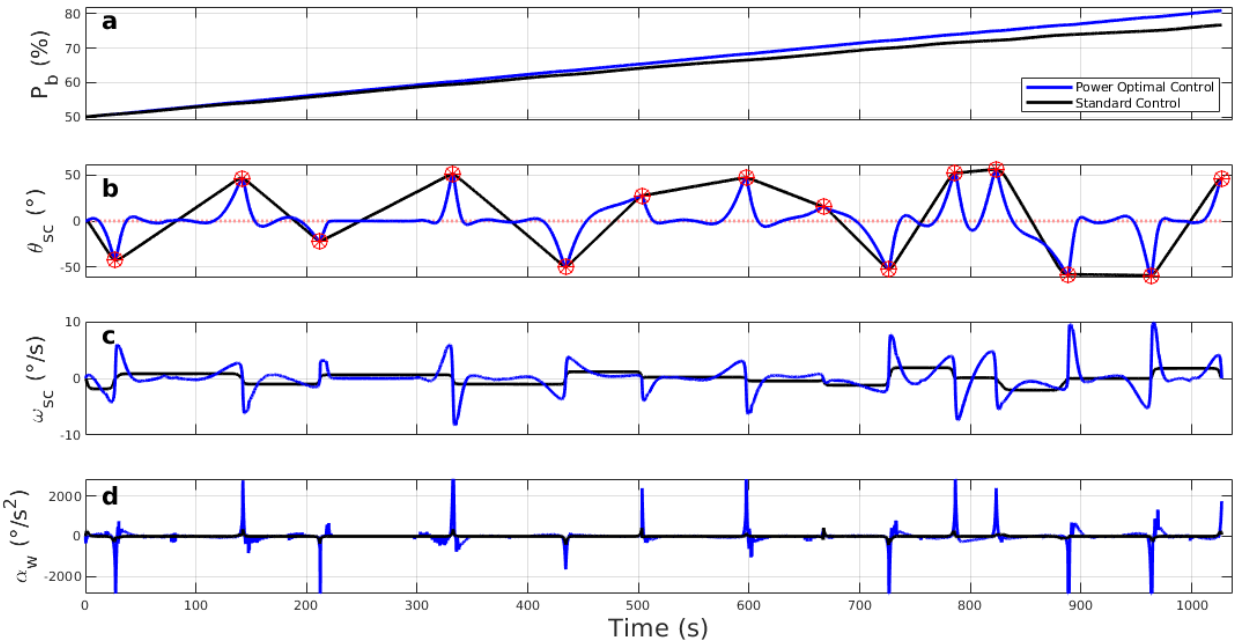

Figure 10: Performance comparison between power-optimal control and standard control for a series of collections. See Figure 6 for explanation of panels and axes. For panel (b), red markers indicate target angles at required times of collection.

timal case expended more power to perform maneuvers; however, the increased power collection more than compensated for the expense. It was determined that sufficient slew time between targets is needed to gain the benefit of power optimization. Additionally, solving for the power state optimal trajectory was found to be more computationally expensive than standard control trajectories. In conclusion, the implementation of a power state optimal control law offers a step toward improved automation and efficiency of satellite maneuvering. Future work is needed to explore additional orbital configurations and to expand the simulation of the satellite and its environment to a full three-dimensional model.

References

[1] K. Lulla, M. D. Nellis, and B. Rundquist, "Celebrating 40 years of landsat program's earth observation accomplishments," 2012.

[2] J. P. Ford, J. B. Cimino, and C. Elachi, "Space shuttle columbia views the world with imaging radar: the sir-a experiment," *NASA STI/Recon Technical Report N*, vol. 83, 1983.

[3] S. Parcak, *Archaeology from Space: How the Future Shapes Our Past*. Henry Holt and Company, 2019.

[4] BlackSky. (2016, Dec.) It's here! introducing the blacksky global intelligence platform. [Online]. Available: https://www.blacksky.com/2016/12/14/its-here-introducing-the-blacksky-global-intelligence-platform/

[5] M. Thompson. (2020, Mar.) First responders in space: How satellites save lives during natural disasters. [Online]. Available: https://www.space.com/43202-earth-satellites-save-lives-natural-disasters.html

[6] E. S. Agency. (2017, Aug.) Sentinel-1 speeds up crop insurance payouts. [Online]. Available: http://www.esa.int/Applications/Observing_the_Earth/Copernicus/Sentinel-1/Sentinel-1_speeds_up_crop_insurance_payouts

[7] DigitalGlobe. (2016, Apr.) Digitalglobe and auracle team up to deepen search capabilities in global mineral exploration. [Online]. Available: http://blog.digitalglobe.com/news/digitalglobe-and-auracle-team-up-to-deepen-search-capabilities-in-global-mineral-exploration/

[8] R. Votel and D. Sinclair, "Comparison of control moment gyros and reaction wheels for small earth-observing satellites," 2012.

[9] D. Adams, D. Bruno, P. Shah, and B. Keller, "Precision control, knowledge and orbit determination on a small spacecraft bus: The orbview-4 attitutde control system," 1998.

[10] T. Shimizu and C. Underwood, "Supercapacitor energy storage for micro-satellites: Feasibility and potential mission applications," *Acta Astronautica*, vol. 85, pp. 138–154, 2013.

[11] J. T. King and M. Karpenko, "A simple approach for predicting time-optimal slew capability," *Acta Astronautica*, vol. 120, pp. 159–170, 2016.

[12] C. Wu, R. Xu, S. Zhu, and P. Cui, "Time-optimal spacecraft attitude maneuver path planning under boundary and pointing constraints," *Acta Astronautica*, vol. 137, pp. 128–137, 2017.

[13] M. Karpenko and J. T. King, "Maximizing agility envelopes for reaction wheel spacecraft," *Proceedings of the Institution of Mechanical Engineers, Part G: Journal of Aerospace Engineering*, vol. 233, no. 8, pp. 2745–2759, 2019.

[14] Y. Hu, B. Wu, Y. Geng, and Y. Wu, "Smooth time-optimal attitude control of spacecraft," *Proceedings of the Institution of Mechanical Engineers, Part G: Journal of Aerospace Engineering*, vol. 233, no. 7, pp. 2331–2343, 2019.

[15] E. A. Culton, "Minimum electrical energy spacecraft maneuvers: Theory and experiments," Naval Postgraduate Scho Monterey United States, Tech. Rep., 2019.

[16] H. Schaub, "Locally power-optimal spacecraft attitude control for redundant reaction wheel cluster," in *AIAA/AAS Astrodynamics Specialist Conference and Exhibit*, 2008, p. 6259.

[17] R. Blenden and H. Schaub, "Regenerative power-optimal reaction wheel attitude control," *Journal of guidance, control, and dynamics*, vol. 35, no. 4, pp. 1208–1217, 2012.

[18] M. Vasquez and J.-K. Hao, "A "logic-constrained" knapsack formulation and a tabu algorithm for the daily photograph scheduling of an earth observation satellite," *Computational optimization and applications*, vol. 20, no. 2, pp. 137–157, 2001.

[19] B. Song, F. Yao, Y. Chen, Y. Chen, and Y. Chen, "A hybrid genetic algorithm for satellite image downlink scheduling problem," *Discrete Dynamics in Nature and Society*, vol. 2018, 2018.

[20] S. Augenstein, A. Estanislao, E. Guere, and S. Blaes, "Optimal scheduling of a constellation of earth-imaging satellites, for maximal data throughput and efficient human management," in *Twenty-Sixth International Conference on Automated Planning and Scheduling*, 2016.

[21] H. D. Curtis, *Orbital mechanics for engineering students*. Butterworth-Heinemann, 2013.

[22] M. J. Sidi, *Spacecraft dynamics and control: a practical engineering approach*. Cambridge university press, 1997, vol. 7.

[23] J. V. Frasch, S. Sager, and M. Diehl, "A parallel quadratic programming method for dynamic optimization problems," *Mathematical Programming Computation*, vol. 7, no. 3, pp. 289–329, 2015.

[24] J. P. Hespanha, *Linear systems theory*. Princeton university press, 2018.